The Importance of Scale in Object-based Mapping of Vegetation Parameters with Hyperspectral Imagery

Elisabeth A. Addink, Steven M. de Jong, and Edzer J. Pebesma

Abstract

In recent years, object-oriented image analysis has been widely adopted by the remote sensing community. Much attention has been given to its application, while the fundamental issue of scale, here characterized by spatial object-definition, seems largely neglected.

In the case of vegetation parameters like aboveground biomass and leaf area index (LAI), fundamental objects are individual trees or shrubs, each of which has a specific value. Their spatial extent, however, does not match pixels in size and shape, nor does it fit the requirements of regional studies. Estimation of vegetation parameters consequently demands larger observation units, like vegetation patches, which are better represented by variably shaped objects than by square pixels.

This study aims to investigate optimal object definition for biomass and LAI. We have data from 243 field plots in our test site in southern France. They cover a vegetation range from landes *to* garrigue *to* maquis*, which is considered to be the climax vegetation in the area. A HyMap image covers the area.*

The image is subjected to a Minimum Noise Fraction (MNF) transformation, after which it is segmented with ten different heterogeneities. The result is ten object sets, each having a different mean object size. These object sets are combined with the original image with the mean band values serving as object attributes.

Field observations are linked to the corresponding objects for each object set. Using Ridge regression, relations between field observations and spectral values are identified. The prediction error is determined for each object set by cross validation. The overall lowest prediction error indicates the optimal heterogeneity for segmentation.

Results show that the scale of prediction affects prediction accuracy, that increasing the object size yields an optimum in prediction accuracy, and that aboveground biomass and LAI can be associated with different optimal object sizes. Furthermore, it is shown that the accuracy of parameter estimation is higher for object-oriented analysis than for per-pixel analysis.

Introduction

Remote sensing data offer a rich information source on vegetation parameters, which may be needed as input to models describing processes at the Earth's surface (Cohen and Goward, 2004). Biomass (e.g., Lu, 2006; De Jong *et al.*, 2003), Leaf Area Index (LAI) (e.g., Weiss and Baret, 1999), and vegetation cover (e.g., Rogan *et al.*, 2002) can reasonably well be estimated with low to moderate resolution imagery (like SPOT-VGT or Landsat TM, respectively). Recently, hyperspectral data added even more power by providing spectral detail that allows detection of some chemical compounds of vegetation (e.g., Kumar *et al.*, 2001; Blackburn, 2002; Haboudane *et al.*, 2002).

The common approach in estimating vegetation parameters is the per-pixel analysis, where field observations are linked to the corresponding pixels to establish the predicting equation. Remote sensing studies on vegetation parameters usually apply a continuous model (Strahler *et al.*, 1986), because the objects of interest are much smaller than the pixels by which they are displayed. Strahler *et al.* (1986) distinguish two types of models depending on the relation between the size of the field objects and the image pixels. The L-resolution models are those models where the scene elements (field objects) are smaller than the resolution cells (pixels), while the H-resolution models includes those models where the pixels are smaller than the field objects. The H-resolution models allow the recognition of individual objects in an image. When the field objects become much smaller than the pixels, they are no longer treated as individual objects but as continuous variables instead. As stated before, this is usually the case for pixel-based vegetation parameter estimation.

When the vegetation is considered as part of a hierarchical scene model (Woodcock and Harward, 1992), the scale and square representation implied by pixels do not fit this model (Fisher, 1997). The natural level would be a vegetation patch with relatively homogenous parameter values. Such a patch will hardly ever be square, so pixels will only sporadically match a natural scale level.

A solution could be found in irregularly shaped observation units, which are never present as such in remote sensing images, but which can be created using image segmentation. This is a procedure in which individual pixels are grouped into spatially continuous regions where the variance of a (group of) variable(s) (to be selected by the user) does not exceed a certain threshold (Haralick and Shapiro, 1985). The final segmentation depends both on the variables included and the threshold value set.

Department of Physical Geography, Faculty of Geosciences, Utrecht University, PO Box 80115, 3508 TC Utrecht, The Netherlands (e.addink@geo.uu.nl).

Photogrammetric Engineering & Remote Sensing
Vol. 73, No. 8, August 2007, pp. 905–912.

0099-1112/07/7308–0905/$3.00/0

Existing segmentation techniques vary (a) in their approach by starting at the entire image which is then subdivided, or starting with the individual pixels which are then grouped, and (b) in the weight given to the spatial component compared to the variables from the feature space (measurement space) (Haralick and Shapiro, 1985). In general, the more accurate results are obtained with the computationally more intensive techniques, i.e., starting with individual pixels and careful selection of the merges to be made (Woodcock and Harward, 1992).

Segmentation studies have been performed for several decades, but only recently computer processing capacity increased such that image segmentation can be implemented with a high level of accuracy and fast performance. This resulted in the development and rapid expansion of object-oriented image analysis (Baatz and Schäpe, 2000). Instead of analyzing the spectral behavior of individual pixels, neighboring pixels are grouped into objects, which then form the observation units. This grouping bypasses the problem of artificially square objects as used in per-pixel analysis (Fisher, 1997), as long as the objects of interest cover a number of pixels allowing a meaningful representation of their shape. Objects can be defined by segmentation, stratification, or a combination of the two. Segmentation was discussed earlier. Stratification is the process of grouping pixels according to an external variable, the detail of which determines the result.

Remote sensing classification studies profit from this latter development. Object-oriented image analysis is much closer to human vision than the per-pixel analysis. Classification studies show both higher accuracy values and more detailed legends (e.g., Yuan and Bauer, 2006).

The application of object-oriented image analysis in vegetation parameter studies has been very limited so far, although it seems to offer improvements on two aspects. First, the geometric inaccuracies in both field and image data are of less importance, since a field plot is linked to an object rather than a pixel. The risk of linking it to a wrong object is much smaller than the risk of linking it to a wrong pixel, because of the larger spatial extent of objects (Mäkelä and Pekkarinen, 2001). Secondly, the remote sensing model changes from a continuous L-resolution model to a continuous H-resolution model, where the objects of interest are larger than a single pixel, but where the label assigned to this object is still a continuous variable. Field plots are often chosen such that they represent a vegetation patch. With per-pixel analysis, this information is ignored, while by grouping pixels, vegetation patches can show as individual objects (depending on the heterogeneity threshold). Besides, by considering segments correlations between bands within a segment can be taken into account as well (Atzberger, 2004).

In literature on segmentation or object-oriented image analysis very little attention is paid to optimal object definition. However, the definition is thought to affect the relations that are found between field observations on vegetation parameters and spectral information (Marceau *et al.*, 1994). Object definition by segmentation comprises both the choice of spectral bands to be considered and the setting of a heterogeneity threshold. With high correlations between adjacent bands, the variance that these bands represent easily gets too much weight. When objects are defined by stratification, the detail of the external variable determines the resulting objects.

Furthermore, optimal object definition need not be identical for different vegetation parameters. For example, biomass and leaf area index (LAI) are subject to different dynamics. Biomass is determined by the accumulation of yearly net growth. Whereas LAI is largely determined by the yearly situation; in the case of evergreens the situation of the previous two to four years will be dominant. Given this difference in temporal steering dynamics, the optimal object definition might also be different.

This paper focuses on the spatial aspects of object definition by segmentation for vegetation parameter estimation, i.e., on the effect that the maximum heterogeneity has. The optimal spatial definition is here defined as the level of segmentation that results in the lowest prediction error of the vegetation parameters. Although the spectral bands definitely will have their effect on object definition as well, this will not be considered here. The aim of this paper is to answer two questions:

1. How does the spatial definition of objects affect the statistical relationships between field observations of leaf area index and aboveground biomass and spectral object properties and what is the optimal spatial definition?
2. Is this effect similar for the vegetation parameters leaf area index and aboveground biomass?

Data

The study area needed to meet two conditions: (a) The natural vegetation should show substantial variation, and (b) hyperspectral data should be available. We selected a study area in the La Peyne catchment in southern France, 60 km west of Montpellier (Figure 1).

Vegetation Data

From August to October 2005 a field campaign was held. Natural land-cover ranges from open areas with low herbaceous vegetation, *landes*, through dense bushes up to 2 m, *garrigue*, to the climax vegetation of the region, *maquis* (Sluiter, 2005; Sluiter and De Jong, 2007). In the literature, *maquis* and *oak forest* are sometimes considered as different vegetation types, distinguished by tree height. In this study both types are considered as *maquis*. The vegetation in the study area frequently suffers from water and heat stress, as in all Mediterranean areas (Archibold, 1995).

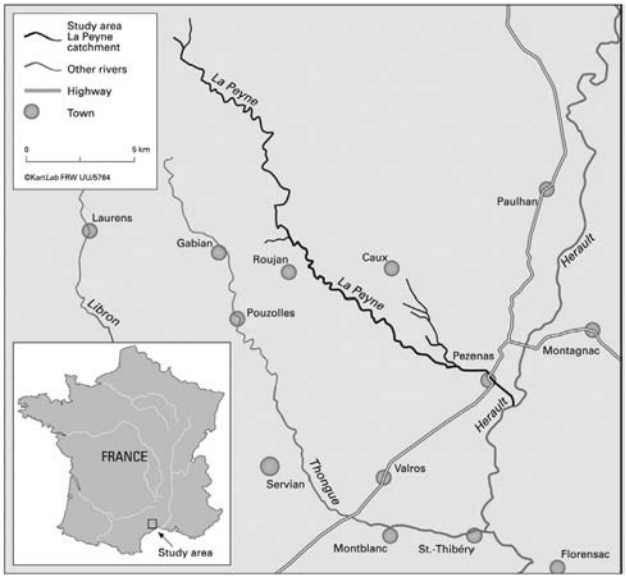

Figure 1. Study area.

The spatial variation of vegetation cover, leaf area index and aboveground biomass is high, while the number of species is limited. Dominant tree species are Holm oak (*Quercus ilex*), Downy oak (*Quercus pubescens*), Kermes oak (*Quercus coccifera*), and the strawberry tree (*Arbutus unedo*). The large spatial variation of the vegetation is caused by the short range variation of geologic formations and soil types resulting in significant, short range differences in water and nutrient availability.

Within the area, 243 plots were sampled. They were distributed over the different vegetation types; within each type nested sampling schemes were applied to ensure spatial randomness and efficiency as most of the vegetation types are hard to access. Distances between the plots within a nest ranged from 10 to 90 m. Several nests coexisted within each vegetation type. Each plot measured 5 m $\times$ 5 m and was sampled for biomass and LAI.

Biomass

Biomass, in general, includes the aboveground and belowground living mass (Lu, 2006). In this study we only consider aboveground biomass, because of the difficulty of collecting belowground biomass data and since aboveground biomass reflects degradation status of ecosystems, a further objective of this study.

Three different approaches exist in aboveground biomass estimation; they are based on field measurements, remote sensing, and GIS-based methods (Lu, 2006). Field measurements provide the most accurate biomass data, but since they are time consuming and labor intensive, it is not viable to use them for large areas. Remote sensing currently forms the primary source for large area aboveground biomass estimation, because of, among other reasons, the synoptic view and proven reasonable correlation between spectral bands and vegetation parameters.

We used allometric formulas to collect field data, which were then related to spectral data. Allometric techniques rely on relationships between a vegetation parameter as such and any dimension(s) of the woody plant element, e.g., stem diameter, tree height, and crown base height (Jonckheere *et al.*, 2004). For trees, we used the following formulas from Ogaya *et al.* (2003):

$$\ln AB = 4.900 + 2.277 \ln D50 \quad (1)$$

$$\ln AB = 3.830 + 2.563 \ln D50 \quad (2)$$

where AB = aboveground biomass (in g), and D 50 = stem diameter at 50 cm (in cm).

Equations 1 and 2 relate to the evergreen oak (*Quercus ilex*) and the strawberry tree (*Arbutus unedo*), respectively. The remaining trees were grouped into two groups based on morphological similarity to either the evergreen oak or the strawberry tree, and the corresponding formulas were applied to them.

For shrubs we used a similar formula provided by Pereira *et al.* (1994):

$$AB = 0.642 \cdot H^{0.0075} \cdot D\,\max^{2.4901} \quad (3)$$

where AB = aboveground biomass (in kg), D max = maximal diameter (in m), and H = height (in m).

Those equations were used to estimate the aboveground biomass for individual trees or shrubs; by summing all results per plot and dividing it by the plot area, values were transformed into the amount of biomass per hectare. Obviously, trees with their stems within a plot can have branches outside the plot and vice versa. We assumed that the biomass estimation error caused by this is negligible.

Biomass data were collected for 216 plots (Table 1).

TABLE 1. STATISTICAL CHARACTERISTICS OF FIELD DATA

	Biomass [Mg/ha]	LAI [-]
N	216	243
mean	167	3.2
sd	209	0.84
variance	43742	0.7
min	0.1	0.4
max	1347	5.4
cv	1.25	0.26

Leaf Area Index

Leaf Area Index is the one-sided leaf area per unit surface area. Direct estimates can be obtained by using a probe and counting how often it hits a leaf when going through the canopy. A destructive alternative includes picking all leaves over a surface unit and scanning their area. An advantage of both methods is the accuracy of the estimates. The first method, however, provides a value for a single point which can vary significantly over short distances. The second method is time-consuming, since every leaf over the plot area needs to be picked individually.

Indirect measurements are based on the light coming through the canopy from different angles. The LAI-2000 Plant Canopy Analyzer (Li-COR, Lincoln, Nebraska) is widely used to determine LAI values *in situ*. The instrument, however, is costly and sensitive to different weather conditions. An alternative can be found in hemispherical photographs. This method is based on classifying the photos into one of two classes; sky or vegetation. For different angles the gap fraction is calculated and combined over the different angles this indicates the LAI. Alternatively, the gap fraction is calculated for a viewing angle of 57.5° as Warren-Wilson (1963 in Weiss *et al.*, 2004) demonstrated that projected area of the leaves (i.e., LAI) at this angle is almost independent of leaf inclination. Hemispherical photos are less costly and less sensitive to weather conditions as well. Advantages of the Licor2000 instrument are the ease and speed with which the measurements are performed. The hemispherical photos require more processing time since they need to be classified, but are much cheaper than the Licor2000. The ease and speed in the field are similar, although the Licor2000 needs reference measurements in the open field which can be cumbersome in forested environments.

Weiss *et al.* (2004) performed a comparing study of methods to determine or estimate LAI. They conclude that calculation of the gap fraction at 57.5° from hemispherical photographs provides the most accurate estimates (RMSE = 0.2) of LAI.

Within this study, we decided to use hemispherical photographs. The sampling strategy within plots is not a very critical issue within continuous canopies (Weiss *et al.*, 2004). We collected five photos, four at the diagonals one meter from each corner and one in the center of the plot. This way the plot was covered evenly, and each tree present in the plot would be represented in at least one photograph. Photos were taken at 50 to 80 cm above the surface. Only photos taken in the upward direction were used, since automatic distinction between vegetation and soil proved impossible in this arid environment. This will result in a slight underestimation for the *garrigue* and *maquis* plots, although the vegetation below 50 cm is usually very thin or even absent. The *landes* plots, where vegetation did not exceed 50 cm, were excluded from the analysis since no LAI data could be collected for them.

For the processing of the photos we used CAN-EYE, a free software package developed at INRA, Avignon (Baret and Weiss, 2004). It calculates the gap fraction for 57.5°. With CAN-EYE first parts of the photos showing the sun or persons were masked out. The remaining parts of the photos were then classified into one of two classes, sky or vegetation. After correcting for vegetation clumping, the LAI values for the five photos were averaged resulting in a plot LAI value.

In total 243 plots were sampled for LAI (Table 1).

Image Data

A HyMap image recorded on 13 July 2003 covers the catchment of the Peyne river. The image has 124 bands and provides continuous spectral cover from 444 to 2,475 nm. The spatial resolution is 5 m. The image was radiometrically processed and geometrically rectified using ground control points determined by GPS in the field and a 25 m resolution DEM with the methods described in Schläpfer and Richter (2002) and Richter and Schläpfer (2002).

Methods

Data Processing

Masking

Since we are interested in vegetation parameters, only the vegetated pixels were included in the analysis to assure that spectral variance in the image is a result of variance in vegetation characteristics only. To remove the non-vegetated pixels, a mask was produced in two steps. First, all pixels with an NDVI value of 0.25 and less were selected. Next, a buffer operation was applied, and the selected pixels were all buffered by two more pixels. Without the buffer, the pixels next to (masked-out) roads would show extreme values in the succeeding Minimum Noise Fraction (MNF) transformation, indicating that they were affected by the neighboring non-vegetated pixels.

Minimum Noise Fraction

In a second step, we needed to reduce the 124-band data set to a smaller number of bands. This need arises because (a) computationally, the segmentation procedure is prohibitively slow for such a large data set, (b) we believe the data contains noise, which can be discarded before the segmentation step, and (c) the 124 bands are highly redundant (collinear). To reduce the data set, we used Minimum Noise Fraction (MNF) transformation (Green *et al.*, 1988; Switzer and Green, 1984). This procedure is an extension to principal components, in the sense that in addition to picking up variance or correlation across bands it tries to capture independent spatial correlation components, i.e., the spatial patterns of interest in the consecutive bands. For the MNF transformation, we used IDL-ENVI, Version 4.1 (RSI, 2004). To estimate the spectral covariance matrix of the noise component, a "homogeneous" region had to be identified; we used a deep artificial lake in the center of the image for this. A set of 20 MNF transformed bands was selected, explaining 84 percent of the total variance in the masked imagery.

Segmentation

Segmentation of the image was performed with eCognition 3.0, an object-based image analysis package (Definiens, 2003), that applies a spatial clustering technique (Haralick and Shapiro, 1985). Objects are formed by pair-wise clustering, beginning with single-pixel objects (Baatz and Schäpe, 2000; Benz *et al.*, 2004). Clustering starts at randomly located seed points with a regular spatial distribution, aiming at maintaining similar object sizes in the image. The clustering procedure stops when the heterogeneity threshold set by the user is exceeded. Heterogeneity can stem from two sources, spectral and shape heterogeneity. The increase in spectral heterogeneity ($\Delta h_{\text{spectral}}$) associated with the merge of two objects (obj_1 and obj_2) is defined as (Benz *et al.*, 2004):

$$\Delta h_{spectral} = \sum_s w_s \left(n_{obj\_merge} \cdot \sigma_{s,merge} - \left(n_{obj\_1} \cdot \sigma_{s,obj\_1} + n_{obj\_2} \cdot \sigma_{s,obj\_2}\right)\right) \quad (4)$$

with s standing for spectral band number, w for weight factor, n for number of pixels in an object, *obj_merge* for the merged object, and σ for the standard deviation within an object. The maximum increase in heterogeneity stemming from the merge of two objects is set by the *scale parameter*.

We defined the objects exclusively by MNF values without any limitations from shape parameters. Since (a) the bands are not normalized, and (b) $\Delta h_{\text{spectral}}$ is not corrected for the number of bands, the meaning of *scale parameter* values are data-set specific. The MNF image was segmented ten times with increments of the scale parameter of 5. The number of segments decreased rapidly with increasing scale parameter values (Table 2 and Plate 1).

TABLE 2. NUMBER OF SEGMENTS (N) RESULTING FROM SEGMENTATION WITH DIFFERENT SCALE PARAMETERS (SCALE)

Scale	N
1 pixel	943966
5	8763
10	3752
15	2800
20	2458
25	2286
30	2203
35	2147
40	2103
50	2067

For each segment, the mean value for each of the 124 HyMap bands was calculated.

Data Set Preparation

For both vegetation parameters, LAI and aboveground biomass, 11 data sets were prepared, ten for the different segmentation levels, and one relating the field plots to individual pixels. As a result 22 data sets were prepared. Each data set contained the parameter values for each plot and the 124 spectral band values, so the number of observations is equal in each data set of the respective parameters (LAI and Biomass). The MNF bands were only used to segment the images, while the relationship between the HyMap image and the vegetation data will be based on the original bands.

Statistical Analysis

Ridge Regression

The relation between the full set of 124 spectral bands on one hand and the vegetation parameters biomass and LAI on the other hand is determined using Ridge regression (Hastie *et al.*, 2001). This is a linear multiple regression method, which searches for the minimum of squared prediction errors, while at the same time limiting the squared sums of the regression coefficients. In situations with many correlated predictor variables, like the spectral bands in hyperspectral images, regression coefficients become poorly determined and exhibit high variance, which is solved by imposing a size constraint, penalty, on the coefficients. The criterion minimized in ridge regression (RSS) is:

$$RSS(\lambda) = \sum_{i=1}^{n} \left(y_i - \hat{y}_i\right)^2 + \lambda \sum_{j=1}^{p} \beta_j^2 \quad (4)$$

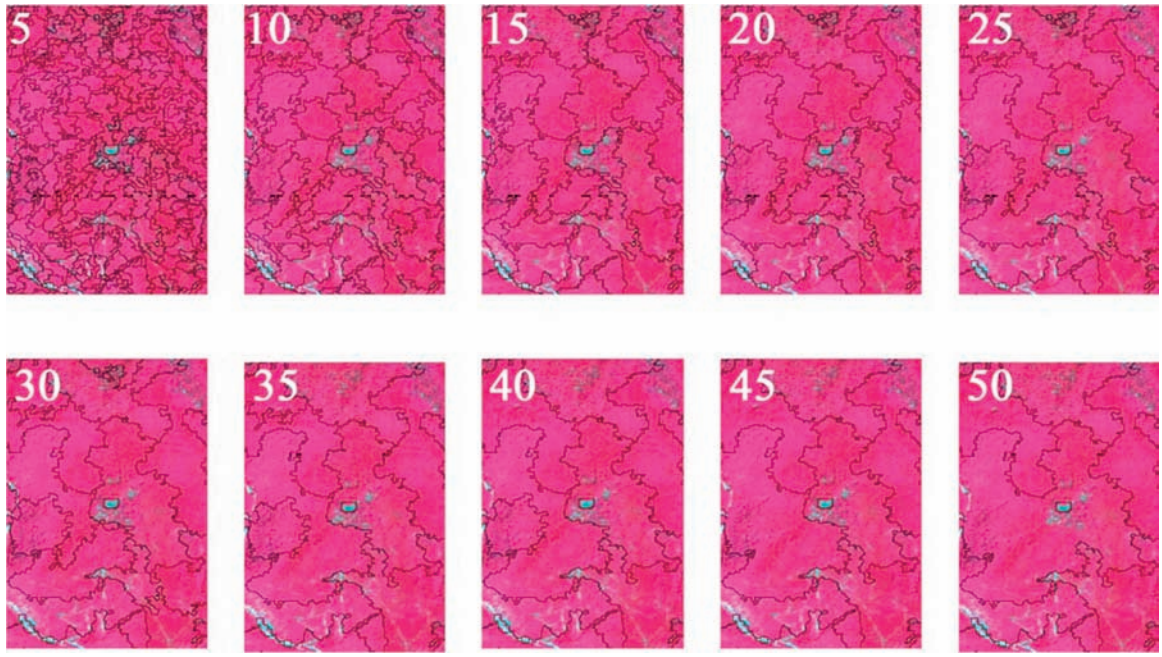

Plate 1. Example of segmentation with different scale parameters (indicated in the upper left corners) overlaid on a subset of the HyMap image (RGB: 783 nm, 662 nm, 539 nm).

where λ controls the amount of shrinkage of the regression coefficients, n is the number of observations, y is the dependent variable and $\hat{y}$ the regression prediction, p is the number of equivalent independent variables (bands), and β_j stands for the j^{th} regression coefficient. It should be noted that the intercept is not penalized, and that predictors are standardized before ridge regression is applied.

The size constraint of the regression coefficients relative to the regression residual sum of squares is determined by λ. There is an inverse, non-linear relation between λ and the effective degrees of freedom (DF) of the regression coefficients. These degrees of freedom can be viewed as the number of independent regression coefficients fitted. With λ equal to 0, ridge regression is equal to ordinary multiple linear regression with df equal to the number of parameters (bands). By increasing λ, DF will decrease (Hastie *et al.*, 2001, p. 63, Equation 3.50). The coefficient λ needs to be tuned using cross validation.

Ridge regression was applied to raw, i.e., non-transformed measurements of LAI and biomass. Some remarks about the potential of transformations will be given in the discussion.

Cross Validation

The optimal value for λ of the Ridge regression functions was determined using generalized cross validation (GCV). GCV is a convenient approximation to leave-one-out cross validation for linear models. GCV values were calculated for each data set for the same range of λ values. The value of GCV is equal to the residual variance, so implying that lower GCV values indicate better performance. Ridge regression and GCV computations were done using (a modified version of) the "ridge.lm" function in the MASS library (Venables and Ripley, 2002) of R, Version 2.3.0 (Ihaka and Gentleman, 1996). The modification addresses the computation of GCV, and can be obtained from the authors.

Distribution of Observations Over Segments

As mentioned above, the observations were collected in the field using a nested sampling approach. The distribution of individual observations over specific segments was not controlled, as the segments were not available ahead of the fieldwork. For small segments (scale parameter 5), the maximum number of observations in a segment amounted to 5, for large segments (scale parameter 50), it amounted to 35. In the statistical analysis no special measures were taken to compensate for the fact that multiple observations could lie in a single segment, as (a) the observations were taken using a nested but still random sampling scheme, and (b) each single observations is expected to contain the same amount of information.

Results

In this study, we investigated the importance of scale of image objects for quantitative mapping of structural vegetation parameters. A Mediterranean study area was carefully selected displaying high spatial variability of vegetation cover, aboveground biomass, and leaf area index, while the number of dominant species was limited to four. The spatial variability of vegetation parameters in this mixed evergreen forest is caused by the short-range variation of geologic substrate and soil resulting in significant differences in water and nutrient availability. The statistical properties of the vegetation illustrate this high variation (Table 1). It is therefore anticipated that the differences between LAI and aboveground biomass found in this study, will also be valid for other areas. The optimal object size is strongly related to the spatial patterns of vegetation, which in turn are dependent on the spatial arrangement of environmental parameters like geologic substrate, soil, and topography. The object size is therefore considered to be site specific.

The results of the cross validation of the Ridge regression are given in Figures 2 and 3 for Leaf Area Index and Biomass, respectively. For both parameters, ten graphs are provided showing from top-left to lower-right, the results for individual pixels to scale parameter 50. For layout reasons, the graphs for scale parameter 45 are not shown. However, in both cases these curves do confirm the trend shown by scale parameters 40 and 50.

The vertical axis shows the GCV values, while the horizontal axis shows the degrees of freedom, DF. The lowest points of the graphs indicate the best performance for a given scale parameter. For Leaf Area Index, scale parameter 15 shows the lowest GCV minimum of the ten graphs in Figure 2. The GCV value of 0.38 corresponds to 54 percent unexplained variance, which means an R^2 of 0.46. For biomass, scale parameter 10 shows the lowest GCV value of the ten graphs in Figure 3. The value of 23000 results in an R^2 of 0.47.

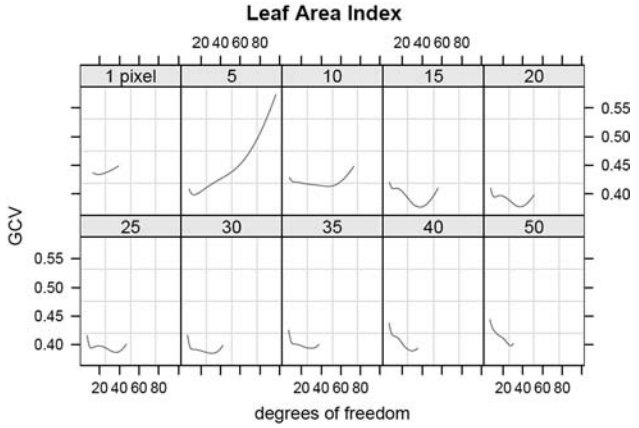

Figure 2. The Generalized Cross Validation (GCV) of Leaf Area Index plotted against the degrees of freedom for 10 different object definitions. GCV is equal to the unexplained variance, lower values indicate better estimates. Each plot corresponds to a scale parameter of Table 2.

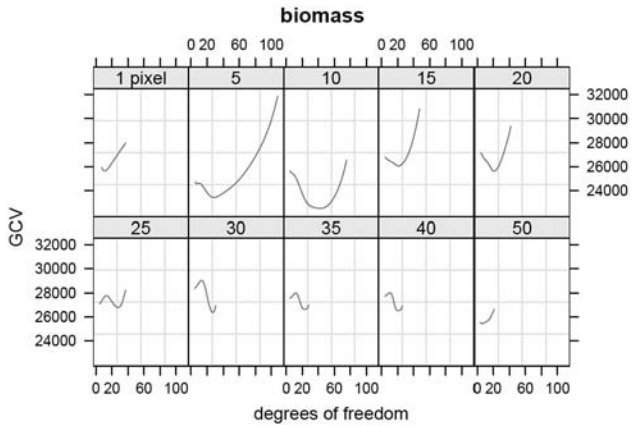

Figure 3. The Generalized Cross Validation (GCV) of aboveground biomass plotted against the degrees of freedom for 10 different object definitions. GCV is equal to the unexplained variance, lower values indicate better estimates. Each plot corresponds to a scale parameter of Table 2.

For biomass (Figure 3), optimal performance increases from individual pixels to scale parameter 10, after which it decreases again with larger scale parameters. For leaf area index the initial trend is not so straightforward, with scale parameter 5 showing better results than scale parameter 10, although the optimum at scale parameters 15 or 20 is clearly better. From 25 on, the performance shows a clear decreasing performance.

Total variance in the independent variables, in this case the spectral bands, determines the relation between the size constraint of the regression coefficients λ, and DF. Lower total variance results in a smaller range of possible DF values. This shows in the smaller range covered by DF with increasing scale parameters (Figures 2 and 3), as the λ values were held constant for all segment sizes, except for the single pixel situation which was run with a smaller λ range.

Discussion

This study relates quantitative field estimates of aboveground biomass and leaf area index with hyperspectral observations acquired with HyMap. The values estimated in the field match the results in other Mediterranean studies. For aboveground biomass, we found values ranging from 0.1 to 1347 Mg ha^{-1} with a mean value of 167 Mg ha^{-1}. Mooney (1981) found 270 Mg ha^{-1} for oak forest while Rapp and Loissant (1981) studied *maquis* with 43.6 Mg ha^{-1}. De Jong *et al.* (2003) found values of 9.5 Mg ha^{-1} for *garrigue*, 73 Mg ha^{-1} for *maquis*, and 169 Mg ha^{-1} for *oak forest*. Very few allometric formulas are available to estimate biomass in natural or Mediterranean vegetation. Given the destructive nature and the complicated logistics of a study to determine them, this is understandable, but it would be satisfying to have more formulas in order to get a better idea of their quality.

The LAI values found in this study, range from 0.4 to 5.4 with an average of 3.2, and a standard deviation of 0.84. These results match well with the mean LAI value of 2.96 found by Caraux Garson and Lacaze (2003) in the Puéchabon area, which is located 40 km NE of the Peyne area in a similar region. Jonckheere *et al.* (2004) give a brief literature review on global LAI values for forests and report values between 0.4 and 16.9, well covering the values found the Peyne area. In general, the highest values are reported for coniferous canopies, which are absent in the Peyne catchment.

The effect of image segment size, i.e., the spectral heterogeneity, on the mapping accuracy of these vegetation parameters is investigated. The study shows that the different levels of segmentation result in different accuracy values for estimation of Leaf Area Index and biomass. Segmentation compared to the one-pixel situation shows that segmentation indeed does provide better estimates, i.e., object-oriented parameter estimation performs better than per-pixel estimation.

By segmenting the images, information is lost. Up to a certain level, this is expected to be noise stemming either from spectral noise or spatial mismatch. Spectral noise can stem from sensor noise, atmospheric influences, or the effects of the point-spread function (Schowengerdt, 1997). At a certain aggregation level, the lost information might turn out to be relevant. This would show in worse results, in our case in higher GCV values. Both phenomena can be observed

in the GCV curves for the different scale parameters. Predictions improved until scale parameter 10 for biomass and until 15 for leaf area index, and decreased with subsequent scale parameter values.

This study does not aim at determining the exact scale parameters that yield optimal predictions, but merely at showing that different heterogeneity values yield different results. The optimal scale parameter could be derived by increasing it with smaller increments. The method used for matching field observations to highly correlated segment characteristics was ridge regression, a variety of linear regression that deals with multi-collinearity. Arguably, this method works best when regression residuals are homoscedastic and independent. Especially for biomass, homoscedasticity is very unlikely and one might suggest to log-transform biomass ahead of the analysis. The interpretation would however change for such a model, and back-transformation of predictions might become an issue. We assumed independence based on the fact that random sampling was used. However, samples were spatially nested, and some spatial correlation is inevitably present. Although part of this is explained by the segment properties, in a more thorough analysis one might suggest to take residual spatial correlation into account.

The optimal scale of observation (i.e., object size with object-oriented image analysis) depends on: (a) the scale of the phenomenon of interest, the processes which are responsible for it and how they can be scaled up, and (b) on the spatial heterogeneity of the landscape. Biomass and leaf area index data were collected on the same plots, so within the same landscape. Still they show different optimal object sizes, implying that their steering processes/factors show different spatial patterns. This is explicable since the LAI of these evergreens is steered by the seasonal cycle of solar radiation and precipitation while actual standing biomass is the result of long-term accumulation of yearly net growth. The optimal pixel size for images from which the objects are derived should be considerably smaller than the optimal object size. The imposed squareness of the pixels (Fisher, 1997) would otherwise prohibit proper representation of the object shapes.

The band setting for the segmentation was held constant in this study by using the first 20 MNF bands for all segmentations. However, different wavelengths show different spatial variances (Atkinson and Aplin, 2004), which will affect object definition. A combination of different object sizes (spectral heterogeneity) with different band combinations was not considered here but will be a future research topic.

Conclusions

In this paper, we studied the effect of increasing heterogeneity in object definition on the accuracy of predicting biomass and leaf area index values from a HyMap image. We used Ridge regression to establish equations and by a leave-one-out cross validation the accuracies of the estimations were determined. We aimed at answering two questions: (a) How does the spatial definition of objects affect the statistical relationships between field observations and spectral object properties? and (b) Is this effect similar for different vegetation parameters?

The values found for aboveground biomass and leaf area index match literature values well, suggesting a more general validity of our conclusions. It is concluded that different heterogeneities indeed result in different estimation accuracy values. Starting with individual pixels and increasing the object size, the predictions improve until an optimum is reached, after which increasing object size results in worse predictions. The question what determines the optimal setting (e.g., landscape heterogeneity, vegetation density, pixel and plot size), is the next issue to study.

Furthermore, our results show that leaf area index and aboveground biomass show different optima for their predictions; aboveground biomass is optimally predicted at scale parameter 10, while leaf area index shows highest prediction accuracy at scale parameter 15. This difference probably reflects the different patterns of their steering processes.

With per-pixel image analysis, working with different scales means working with differently sized squares. Both the surface objects reflected in an image and the spectral bands of that image may, and usually will, display a variation of optimal sizes, while the shape of the surface objects hardly ever is square. Now with object-oriented image analysis, the fixed shape and the uniform size of the image objects has been eliminated, but the number of possible tessellations has increased infinitely. Here lies a major challenge for image analysts.

Acknowledgments

This research was financed by the Research Council for Earth and Life Sciences (ALW) of the Netherlands Organization for Scientific Research (836.03.010). Wiebe Nijland, Rogier de Jong, and Paul Hiemstra are greatly acknowledged for their contribution to the field campaign.

References

Archibold, O.W., 1995. *Ecology of World Vegetation*, London, Chapman & Hall, 510 p.

Atkinson, P.M., and P. Aplin, 2004. Spatial variation in land cover and choice of spatial resolution for remote sensing, *International Journal of Remote Sensing*, 25(18):3687–3702.

Atzberger, C., 2004. Object-based retrieval of biophysical canopy variables using artificial neural nets and radiative transfer models, *Remote Sensing of Environment*, 93(1–2):53–67.

Baatz, M., and A. Schäpe, 2000. Multiresolution segmentation - An optimization approach for high quality multi-scale image segmentation, *Angewandte Geographische Informations-Verarbeitung XII* (J. Strobl, T. Blaschke, and G. Griesebner, editors), Karlsruhe, Wichmann Verlag, pp. 12–23.

Baret, F., and M. Weiss, 2004. CAN_EYE: Processing digital photographs for canopy structure characterization - Tutorial, URL: *http://www.avignon.inra.fr/can_eye/* (last date accessed: 19 May 2007).

Benz, U.C., P. Hofmann, G. Willhauck, I. Lingenfelder, and M. Heynen, 2004. Multi-resolution, object-oriented fuzzy analysis of remote sensing data for GIS-ready information, *ISPRS Journal of Photogrammetry and Remote Sensing*, 58(3–4):239–258.

Blackburn, G.A., 2002. Remote sensing of forest pigments using airborne imaging spectrometer and LIDAR imagery, *Remote Sensing of Environment*, 82(2–3):311–321.

Caraux Garson, D., and B. Lacaze, 2003. Monitoring leaf area index of Mediterranean oak woodlands: Comparison of remotely-sensed estimates with simulations from an ecological process-based model, *International Journal of Remote Sensing*, 24(17):3441–3456.

Cohen, W.B., and S.N. Goward, 2004. Landsat's role in ecological applications of remote sensing, *BioScience*, 54(6):535–545.

De Jong, S.M., E.J. Pebesma, and B. Lacaze, 2003. Above-ground biomass assessment of Mediterranean forests using airborne imaging spectrometry: The DAIS Peyne experiment, *International Journal of Remote Sensing*, 24(7):1505–1520.

Definiens, 2003. eCognition, *Object-based Image Analysis*, München.

Fisher, P., 1997. The pixel: A snare or a delusion, *International Journal of Remote Sensing*, 18(3):679–685.

Haboudane, D., J.R. Miller, N. Tremblay, P.J. Zarco-Tejada, and L. Dextraze, 2002. Integrated narrow-band vegetation indices for prediction of crop chlorophyll content for application to precision agriculture, *Remote Sensing of Environment*, 81(2–3):416–426.

Haralick, R.M., and L.G. Shapiro, 1985. Image segmentation techniques, *Computer Vision, Graphics, and Image Processing*, 29:100–132.

Hastie, T., R. Tibshirani, and J. Friedman, 2001. *The Elements of Statistical Learning, Data Mining, Inference, and Prediction*, New York, Springer, 533 p.

Ihaka, R., and R. Gentleman, 1996. R: A language for data analysis and graphics, *Journal of Computational and Graphical Statistics*, 5(3):299–314.

Jonckheere, I., S. Fleck, K. Nackaerts, B. Muys, P. Coppin, M. Weiss, and F. Baret, 2004. Review of methods for in situ leaf area index determination, Part I: Theories, sensors and hemispherical photography, *Agricultural and Forest Meteorology*, 121(1–2): 19–35.

Kumar, L., K. Schmidt, S. Dury, and A.K. Skidmore, 2001. *Imaging Spectrometry and Vegetation Science, Imaging Spectrometry: Basic Principles and Prospective Applications* (F.D. Van der Meer and S.M. De Jong, editors), Dordrecht, Kluwer: pp. 111–155.

Lu, D., 2006. The potential and challenge of remote sensing-based biomass estimation, *International Journal of Remote Sensing*, 27(7):1297–1328.

Mäkelä, H., and A. Pekkarinen, 2001. Estimation of timber volume at the sample plot level by means of image segmentation and Landsat TM imagery, *Remote Sensing of Environment*, 77(1): 66–75.

Marceau, D.J., P.J. Howarth, and D.J. Gratton, 1994. Remote sensing and the measurement of geographical entities in a forested environment, 1: The scale and spatial aggregation problem, *Remote Sensing of Environment*, 49(2):93–104.

Mooney, H.A., 1981. Primary production in Mediterranean-climate regions, *Ecosystems of the World 11: Mediterranean Shrublands* (F. Di Castri, editor), Amsterdam, Elsevier: pp. 249–255.

Ogaya, R., J. Peñuelas, J. Martínez-Vilalta, and M. Mangirón, 2003. Effect of drought on diameter increment of Quercus ilex, Phillyrea latifolia, and Arbutus unedo in a holm oak forest of NE Spain, *Forest Ecology and Management*, 180(1–3):175–184.

Pereira, J.M.C., T.M. Oliveira, and J.P.C. Paul, 1994. Fuel mapping in a Mediterranean shrubland using Landsat TM imagery, *Proceedings of the International Workshop on Satellite Technology and GIS for Mediterranean Forest Mapping and Fire Management* (P.J. Kennedy and M. Karteris, editors), Thessaloniki, Greece, Luxembourg, Office for official publication of the European Communities, pp. 97–106.

Rapp, M., and P. Lossaint, 1981. Some aspects of mineral cycling in the Garrigue of southern France, *Ecosystems of the World 11: Mediterranean Shrublands* (F. Di Castri, editor), Amsterdam, Elsevier, pp. 1289–1300.

Richter, R., and D. Schläpfer, 2002. Geo-atmospheric processing of airborne imaging spectrometry data, Part 2: Atmospheric/topographic correction, *International Journal of Remote Sensing* 23(13):2631–2649.

Rogan, J., J. Franklin, and D.A. Roberts, 2002. A comparison of methods for monitoring multitemporal vegetation change using Thematic Mapper imagery, *Remote Sensing of Environment*, 80(1):143–156.

RSI, 2004. *ENVI - The Environment for Visualizing Images*, Version 4.1, Boulder, Colorado.

Schläpfer, D., and R. Richter, 2002. Geo-atmospheric processing of airborne imaging spectrometry data, Part 1: Parametric orthorectification, *International Journal of Remote Sensing*, 23(13): 2609–2630.

Schowengerdt, R.A., 1997. *Remote Sensing - Models and Methods for Image Processing*, Boston, Academic Press, 522 p.

Sluiter, R., 2005. *Mediterranean Land Cover Change - Modelling and Monitoring Natural Vegetation Using GIS and Remote Sensing*, Utrecht, KNAG, 145 p.

Sluiter, R., and S.M. De Jong, 2007. Spatial patterns of Mediterranean land abandonment and related land cover transitions, *Landscape Ecology*, 22(4):559–576.

Strahler, A.H., C.E. Woodcock, and J.A. Smith, 1986. On the nature of models in remote sensing, *Remote Sensing of Environment*, 20:121–139.

Switzer, P., and A.A. Green, 1984. *Min/max Autocorrelation Factors for Multivariate Spatial Imagery*, Technical Report, Department of Statistics, Stanford University, 6:10 p.

Venables, W.N., and B.D. Ripley (editors), 2002. *Modern Applied Statistics with S*, New York, Springer.

Warren-Wilson, J., 1963. Estimation of foliage denseness and foliage angle by inclined point quadrats, *Australian Journal of Botany*, 11:95–105.

Weiss, M., and F. Baret, 1999. Evaluation of canopy biophysical variable retrieval performances from the accumulation of large swath satellite data, *Remote Sensing of Environment*, 70(3): 293–306.

Weiss, M., F. Baret, G.J. Smith, I. Jonckheere, and P. Coppin, 2004. Review of methods for in situ leaf area index (LAI) determination, Part II: Estimation of LAI, errors and sampling, *Agricultural and Forest Meteorology*, 121(1–2):37–53.

Woodcock, C., and V.J. Harward, 1992. Nested-hierarchical scene models and image segmentation, *International Journal of Remote Sensing*, 13(16):3167–3187.

Yuan, F., and M.E. Bauer, 2006. Mapping impervious surface area using high resolution imagery: A comparison of object-based and per pixel classification, *Proceedings of the ASPRS Annual Conference*, Reno, Nevada.